THE JOURNAL OF PHYSICAL CHEMISTRY B

Article

pubs.acs.org/JPCB

The Behavior of Ionic Liquids under High Pressure: A Molecular Dynamics Simulation

Yuling Zhao,[†,‡] Xiaomin Liu,[‡] Xingmei Lu,[*,‡] Suojiang Zhang,[‡] Jianji Wang,[*,†] Hui Wang,[§] Gabriela Gurau,[§] Robin D. Rogers,[*,§] Lei Su,[∥] and Haining Li[∥]

[†]School of Chemistry and Environmental Science, Key Laboratory of Green Chemical Media and Reactions, Ministry of Education, Henan Normal University, Xinxiang, Henan 453007, China

[‡]Beijing Key Laboratory of Ionic Liquids Clean Process, State Key Laboratory of Multiphase Complex Systems, Institute of Process Engineering, Chinese Academy of Sciences, Beijing, 100190, China

[§]Center for Green Manufacturing and Department of Chemistry, The University of Alabama, Tuscaloosa, Alabama, 35487-0336, United States

[∥]The High Pressure Research Center of Science and Technology, Zhengzhou University of Light Industry, Zhengzhou 450002, China

Supporting Information

ABSTRACT: The effect of pressure on the structure, interionic interactions, and properties of the ionic liquid (IL) 1-butyl-3-methylimidazolium hexafluorophosphate ([C_4mim][PF_6]) was studied using an all-atom molecular dynamics simulation. A distinct conformational transition from anti (*a*) to gauche (*g*) form based on the deformation of the first C−C bond of the butyl chain was observed under high pressure, and the ratio of the *a* conformation that changed into the *g* conformation was 5.5% at 6000 bar. Under high pressure, the configuration of the *a* and *g* conformer for [C_4mim]$^+$ tends to make the alkyl chain distorted to the inside of the ring. Results on the density changes indicate a small increase from 5000 to 6000 bar, which could be attributed to the writhing of the reducing end of the alkyl chain in the cation at higher pressure. These simulation results are well agreed with the experimental results. Transport properties were also calculated at different pressures. The results show that diffusion of the ions is reduced under high pressure, and the viscosity is dramatically enhanced.

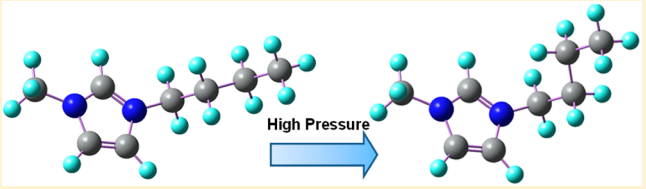

1. INTRODUCTION

Ionic liquids (ILs; salts which melt below 100 °C[1−4]) have been gaining widespread attention recently as a result of the various accessible property sets, such as negligible vapor pressure, nonflammability, thermal and chemical stability, structural tunabilities, and recyclability. The structures of ILs are flexible and can be designed according to the needs of specific applications, which has resulted in ILs being widely considered for diverse applications, including drug delivery or as active pharmaceutical ingredients,[5,6] solvents for green processing of insoluble biomolecules,[7,8] and novel electrolytes for energy applications.[9] With such intense scrutiny worldwide, the reaction conditions of the systems involving ILs are becoming more and more extreme. Thus, it is necessary to study the behavior and properties of ILs under severe conditions. The effects of high pressure,[10] low temperature, high electric fields, and magnetic fields[11,12] on IL properties have been reported.

Su et al.[13,14] reported that 1-butyl-3-methylimidazolium hexafluorophosphate ([C_4mim][PF_6]) experienced a liquid−solid phase transition at about 5000 bar, and Russina et al.[15] studied the structural organization and phase behavior of this IL using high pressure Raman spectroscopy. Domanska et al.[16] studied the solid−liquid phase equilibrium in binary IL mixtures and discussed the solubility changes of ILs under high pressure. Salvador et al.[17] found that cellulase activity in [C_4mim]Cl under pressure is improved compared to that under atmospheric pressure. These studies indicate that high pressure can lead to a phase transition which has an impact on the properties of ILs. Therefore, understanding the behavior of ILs under high pressure will facilitate the expansion of the application of ILs to a variety of new fields.

Pressure can shorten the distance between atoms of ILs, resulting in the changes of the electronic structure and interactions.[18] The attractive force among ions of opposite charge as well as the repulsive interactions among ions of the same charge will increase as pressure increases.[19] The nature of the individual ion structures within an IL will have an effect on the enhancement of such interactions. Chang et al.[20,21] found conformational changes of the butyl chain in [C_4mim]Cl above a pressure of 3000 bar by using high-pressure infrared spectroscopy. Yoshimura and co-workers[19,22,23] reported the structural transition of three typical ILs, [C_4mim][BF_4], [C_4mim][PF_6], and [DEME][TFSI] (*N*,*N*-diethyl-*N*-methyl-*N*-(2-methoxyethyl)ammonium bis(trifluoromethylsulfonyl)-

Received: March 2, 2012
Revised: August 10, 2012
Published: August 11, 2012

   dx.doi.org/10.1021/jp3070568 | *J. Phys. Chem. B* 2012, 116, 10876−10884

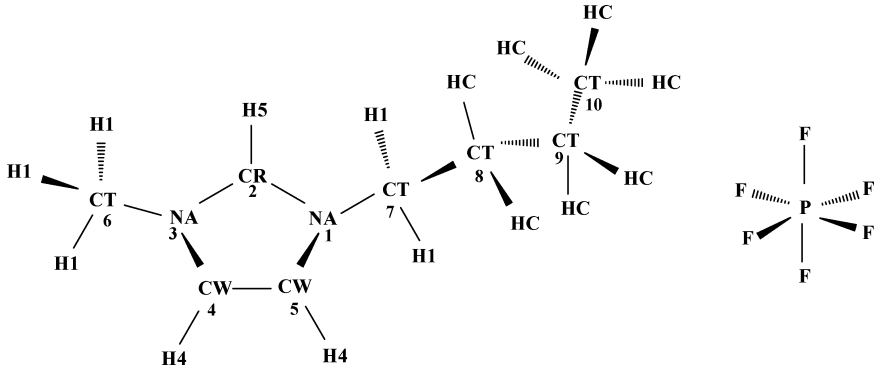

Figure 1. Structure and numbering scheme for $[C_4mim][PF_6]$.

imide), at room temperature under different pressure ranges, where the CH stretching of the alkyl chain in their FT-IR spectra changed significantly at high pressures. For example, the observance of the gauche conformer of the $[C_4mim]^+$ cation in $[C_4mim][PF_6]$ increased with a corresponding decrease in the trans conformer.

Such structural changes in ILs produce changes in the properties under high pressure. For example, Kanakubo et al.[24,25] studied the effect of pressure on the transport properties of 1-alkyl-3-methylimidazolium salts, and found that the electrical conductivity and self-diffusion coefficients of the cation and anion significantly decrease to 20% of their atmospheric pressure values when the pressure was increased to 2000 bar. The viscosity of the ILs increased as the ion diffusion decreased under these conditions.

The above studies suggest that the structure, interactions, and dynamic properties of ILs will change under high pressure; however, there are only a few reports on the effect of pressure on IL structure and properties at the molecular level. Molecular dynamics (MD) simulation is an effective method in the study of liquid molecular structure and dynamics properties. Using MD simulations, the CHARMM,[26] AMBER,[27,28] OPLS,[29,30] and GROMOS[31] force fields of $[C_4mim][PF_6]$ have been developed respectively in previous years. Recently, Zhao et al.[32] examined the nature, mobility, and lifetime of liquid $[C_4mim][PF_6]$. Müeller-Plathe and Balasubramanian et al.[33] studied the correlation between dynamic heterogeneity and local structure of $[C_4mim][PF_6]$ in the temperature range 250−450 K. For MD study of high pressure, Aragones et al.[34] used this method to study the phase diagram of water at high pressures where spontaneous freezing of the liquid into a solid phase at pressures of about 80 000 bar was observed. Kohno et al.[35] reported the effect of high pressure on the crystal structure of 1,3-diamino-2,4,6-trinitrobenzene and a unique structural change was found around 75 000 bar by molecular simulation. Meher et al.[36] have studied the effect of pressure on the conformation and dynamics of HIV-1 protease at 1 and 3000 bar pressure conditions using an AMBER force field. It was clear that turns and bends are favored under high pressure, resulting in the reduction of structural variability from the secondary structure analysis. Velardez et al.[37] calculated the melting temperatures for pressures up to 8000 bar by using an AMBER force field, and found that the computed dependence of the melting temperature on pressure was in excellent agreement with experiment results. Maginn et al.[38] found that the motion of the ions 1-octadecyl-3-methylimidazolium bis(trifluoromethanesulfonyl)imide, $[C_{18}mim][Tf_2N]$, and 1-oleyl-3-methylimidazolium (9,10-*cis*-octadecenyl) bis-(trifluoromethanesulfonyl)imide, $[C_{18}(1[9])mim][Tf_2N]$, is severely retarded at low temperatures and high pressures.

Here, we report the effect of pressure on the structure and interionic interactions of the IL $[C_4mim][PF_6]$, which can be regarded as a typical member of the imidazolium-based ILs, using an all-atom molecular dynamics simulation method. Molecular dynamics simulations were performed for $[C_4mim][PF_6]$ at 313 K under pressures up to 6000 bar. The structure conformation of the imidazolium ring and long alkyl chain was simulated. The interaction energy and transport properties were also calculated to clarify the interactions and dynamic behavior under different pressures. These results were compared with those under normal pressure and with conformational changes to provide physical insight into the nature of the IL phase transitions.

2. SIMULATION METHODOLOGY

A series of MD simulations were performed on $[C_4mim][PF_6]$ (Figure 1) with the M.Dynamix 5.2 package[39] at 313 K with the pressure varying from 1 to 6000 bar using an all-atom Amber force field. The Amber force field framework (eq 1) is shown as follows:

$$U = \sum_{\text{bonds}} K_r(r - r_0)^2 + \sum_{\text{angles}} K_\theta(\theta - \theta_0)^2 + \sum_{\text{torsions}} \frac{K_\phi}{2}(1 + \cos(n\phi - \gamma)) + \sum_{i=1}^{N}\sum_{j=i+1}^{N}\left\{4\varepsilon_{ij}\left[\left(\frac{\sigma_{ij}}{r_{ij}}\right)^{12} - \left(\frac{\sigma_{ij}}{r_{ij}}\right)^{6}\right] + \frac{q_i q_j}{r_{ij}}\right\} \quad (1)$$

The first three terms represent the bonded interactions, i.e., bonds, angles, and torsion angles. The nonbonded interactions are described in the last term, including van der Waals and Coulombic interactions of atom-centered point charges. The force field parameters for $[C_4mim]^+$ cations and $[PF_6]^-$ anions were from Liu's work.[27] Optimization of the isolated ion structures was performed using the Gaussian 03 package at the B3LYP/6-31+G* level. The optimized geometries were used to set equilibrium bond lengths (r_0) and angles (θ_0). Atom charges were obtained by fitting the electrostatic potential calculated at the B3LYP/6-311++G* level, and the one-conformation, two-step restraint electrostatic potential method was used for atom charges.

As the face centered cubic (FCC) type has been used in many reports,[27,40,46,47] all of our simulations started from an

dx.doi.org/10.1021/jp3070568 | J. Phys. Chem. B 2012, 116, 10876−10884

FCC lattice in order to mix the cations and anions evenly; each system contained 256 ion pairs. Periodic boundary conditions were applied with Ewald summation of the electrostatic interactions for the IL. After the system was energy-minimized using a microcanonical ensemble for 5000 MD steps to remove possible overlap in the initial configuration, the NpT ensemble[41] was then adopted and the system density gradually increased to a reasonable value. The temperature and pressure were controlled by a Nosé–Hoover thermostat and barostat,[47] with update frequencies of 0.03 and 0.7 ps, respectively. A 2/0.2 fs multiple time-step algorithm was adopted. The intramolecular forces were cut off at 15 Å, while the long-range forces including LJ and Coulombic interactions were cut off at 20 Å. The system was equilibrated for at least 4 ns by the NpT ensemble, making sure that the system configuration was stable, and then, the structures and properties were calculated over a period of 2.0 ns. Trajectories were dumped in an interval of 10 fs for further analysis. Each test was run three times and took the average to reduce the error.

Additional simulations were carried out to consider the effect of the number of ion pairs and coupling factors on our results (Table S1, Supporting Information). By comparing the densities of the three groups in Table S1 (Supporting Information), it is seen that the effect of these two factors on the density is small. We also conducted an experiment to prove our simulation result. The Raman spectra of $[C_4mim][PF_6]$ were measured at 313 K with different pressures; please see the experimental details in ref 42.

3. RESULT AND DISCUSSION

3.1. Liquid Densities. The calculated liquid densities of $[C_4mim][PF_6]$ at different pressures are shown in Figure 2. The

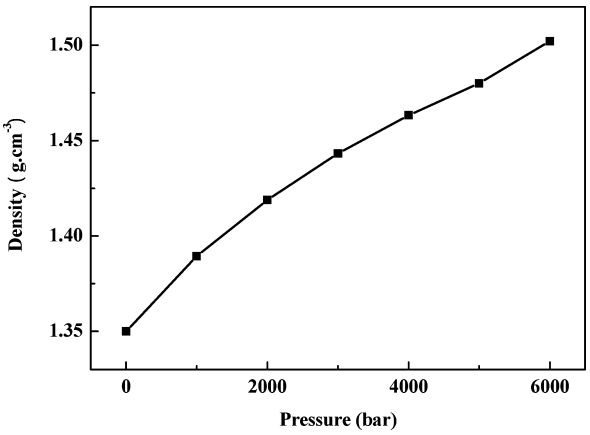

Figure 2. Liquid densities for $[C_4mim][PF_6]$ simulated at different pressures.

computed density at 313 K under normal pressure is 1.350 g/cm^3, which is close to the experimental[43] results of 1.3549–1.3550 g/cm^3. The density values at 1000 and 2000 bar at 313 K are 1.389 and 1.419 g/cm^3, which are close to the reported experimental values[43] of 1.3978 (1000 bar) and 1.4299 g/cm^3 (2000 bar) at 323 K. Compared with the density at atmospheric pressure, that at 6000 bar is 11% higher.

The calculated density gradually increases with increasing pressure at 313 K from 1 to 5000 bar, while it jumps from 1.480 g/cm^3 at 5000 bar to 1.502 g/cm^3 at 6000 bar, which might indicate a phase transition in the IL. Raman spectroscopy was used to characterize $[C_4mim][PF_6]$ under high pressure at 313 K, and the low frequency portion of the spectra are shown in Figure 3. It is clear that the Raman bands have changed when

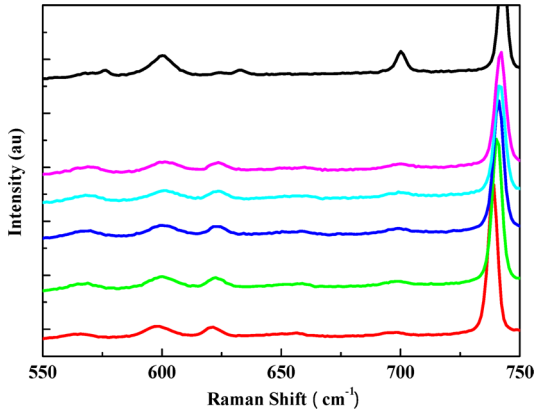

Figure 3. Low frequency portion of the Raman spectra of $[C_4mim][PF_6]$ at 313 K at different pressures: (from bottom to top) 1 bar (red), 2191 bar (green), 3333 bar (blue), 4382 bar (baby blue), 4980 bar (pink), 5700 bar (black).

the pressure is up to 5700 bar, indicating that the phase change of $[C_4mim][PF_6]$ occurs between 4980 and 5700 bar. Many studies[13,15,29] reported that the Raman bands at ca. 600 and 700 cm^{-1} are considered as the fingerprints of the gauche conformation of the side butyl chain. This implies that the ratio of the *g* conformer increases with increasing pressure. This experimental result is consistent with the simulation result. The conformation change will be further discussed in the next section.

3.2. Conformational Change of $[C_4mim]^+$ under Pressure. The study of $[C_4mim][PF_6]$ by Su et al. showed that the peaks of this IL shifted at a pressure under which the IL experienced a phase transition.[13] That study suggested that the structural changes in the crystalline and liquid states under high pressure are associated with conformational changes in the butyl chain, while the anions were essentially unchanged due to their spherical structure. Therefore, here we will focus on the conformation of the $[C_4mim]^+$ cations by analysis of radial distribution functions (RDFs) and torsion angle distributions.

3.2.1. The Effect of Pressure on the Ring. The torsion angle 1–2–3–4 (Figure 1) was calculated at 1 and 6000 bar to determine if there is any deformation of the imidazolium plane. As shown in Figure 4, there was no obvious change in this torsion angle 1–2–3–4 at high pressure, indicating that the ring atoms are planar throughout the pressures studied.

To measure any changes in the inter-ring distances (packing), pair–pair radial distribution function analyses at 1 and 6000 bar were carried out for ring atoms C2, C4, and C5 (Figure 5a) and for these atoms with the phosphorus atom of the anion (Figure 5b). The solid lines represent results obtained at P = 1 bar, while the dotted lines are those obtained at P = 6000 bar. The results suggest that the distances between the rings are reduced at high pressure. It seems that there is only a slight reduction in ring–anion distance. Thus, it suggested that the structure of butyl chain on the ring changed a lot under high pressure.

3.2.2. The Effect of Pressure on the Alkyl Chain. Two different conformations of the side butyl chain have been observed at room temperature, in one form the butyl group is

dx.doi.org/10.1021/jp3070568 | J. Phys. Chem. B 2012, 116, 10876–10884

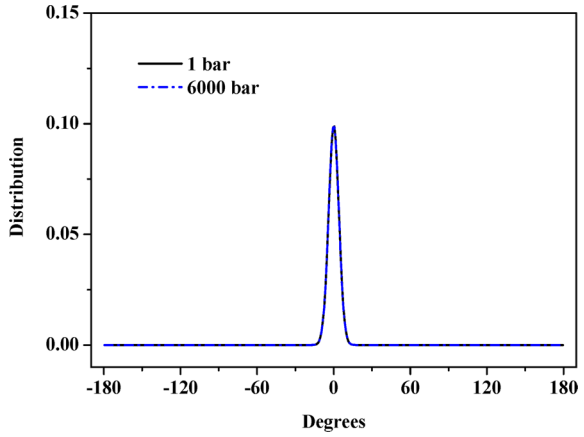

Figure 4. Distribution of torsion angle 1−2−3−4 at 1 and 6000 bar.

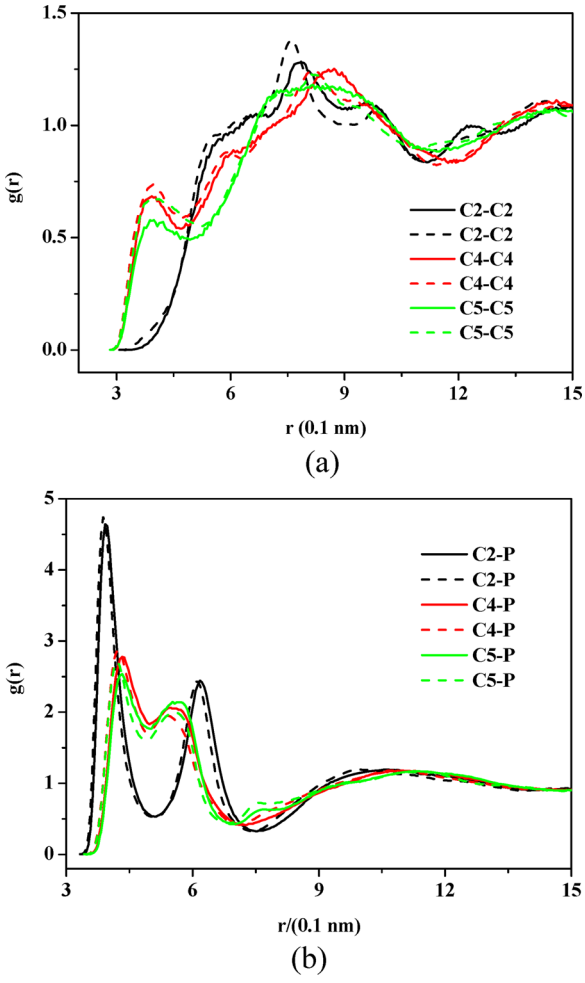

Figure 5. (a) Pair−pair RDFs of C2, C4, and C5 at 313 K. (b) RDFs of C2, C4, and C5 with the phosphorus atom of the anion at 313 K.

anti (*a*, as defined by 1−7−8−9, Figure 1), while in the other the chain is gauche (*g*).[21] On the basis of Raman spectra reported by many groups,[13,15,44] the $[C_4mim]^+$ cation in the liquid state is characterized by the coexistence of the *a* and *g* conformers of the alkyl chain. The schematic diagram is shown in Figure 6. Both of the two conformations were observed in our study.

To further probe the structural changes of these two forms, the distributions of torsion angles among the carbons in the alkyl chains with reference to the imidazolium rings (4−5−1−7, 4−5−1−8, 4−5−1−9, and 4−5−1−10) were calculated at 1 and 6000 bar (Figure 7). From the data, it is clear that there is no obvious change in the 4−5−1−7 torsion angle as the pressure increases, which is expected since C7 is bonded directly to the imidazolium ring. However, the torsion angles for C8 (4−5−1−8), C9 (4−5−1−9), and C10 (4−5−1−10) do change significantly at high pressure. This suggests that the C8, C9, and C10 carbon atoms are easily compressed under high pressure, especially for those that are further from the ring: C9 and the terminal methyl group C10. In Figure 7c, the peaks at ca. ±160° and ca. ±120° stand roughly for *a* and *g* conformers, respectively. The presenting data in this figure shows that the peak height of the *a* conformer decreases while the peak height of the *g* conformer increases. This suggests that a part of the *a* conformer has transformed to the *g* conformer. It means that the configuration of the *a* and *g* conformers for $[C_4mim]^+$ tends to make the alkyl chain distorted to the inside of the ring under high pressure.

The ratio of the *g* conformer was calculated at different pressures in the simulation to investigate the structural changes. The ratio of the *g* conformer was 0.374 at 1 bar which is very close to what Lopes et al. reported[29] (0.38). The increment ratios of the *g* conformer with pressure are shown in Figure 8 and compared with the experimental data reported by Russina et al.[15] From this figure, we can see the increment ratio of the *g* conformer increases with increasing pressure, which is in agreement with the experimental result. This indicates that the *a* conformer decreases and the *g* conformer increases at 6000 bar. Compared with the *g* form at 1 bar, that at 6000 bar increases by about 5.5%.

A small jump in the calculated density from 5000 to 6000 bar suggested that a structural change in this pressure range should be observed. To determine this, the pair−pair RDFs and torsion angles were examined between 5000 and 6000 bar. The data for C7−C7, C8−C8, C7−P, and C8−P in Figure 9a and c indicate only minor changes in the RDFs of C7 and C8 in the first solvation shell; however, larger changes in the configurations are observable for C9 and C10 (Figure 9b and d).

To further study these configuration changes, the distributions of the 7−8−9−10 and 1−7−8−9 torsion angles at 5000 and 6000 bar were calculated (Figure 10). The 1−7−8−9 torsion angles (Figure 10a) showed the change of the ±*g* conformer (±60°), and this configuration is considered to be in the *g* conformer around the C7−C8 bond. The 7−8−9−10 torsion angles (Figure 10b) showed the ±*g* conformer according to the second C8−C9 bond. It is found that the distribution of ±*g* according to the C7−C8 and C8−C9 bonds changed a lot compared with that of the *a* configuration. The ratio of the *a*, −*g*, and +*g* conformers for the butyl chain are also calculated (Table 1) to observe this conformational change. From Table 1, it can be seen that the ratio of the ±*g* conformer for the C7−C8 bond and the +*g* conformer for the C8−C9 bond increase at 5000 and 6000 bar, while the other configuration decreases. This indicates that the C9 and C10 position in the *g* conformer tends to change direction, resulting in a more compact cation (Figure 11) with the terminal methyl group more directly under the ring, leading to the observed jump in density between 5000 and 6000 bar.

The above results indicate that the long alkyl chain is easily compressed under pressure and the cation becomes smaller in order to decrease spatial volumes. On the basis of these results, it is speculated that an even more dramatic effect would be

dx.doi.org/10.1021/jp3070568 | J. Phys. Chem. B 2012, 116, 10876−10884

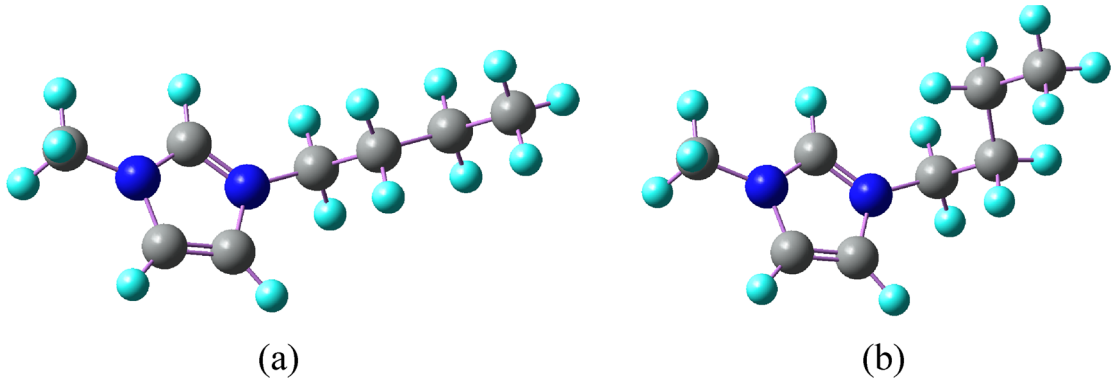

Figure 6. The *a* (a) and *g* (b) forms of $[C_4mim]^+$ in the simulated system as defined by torsion angles 1−7−8−9.

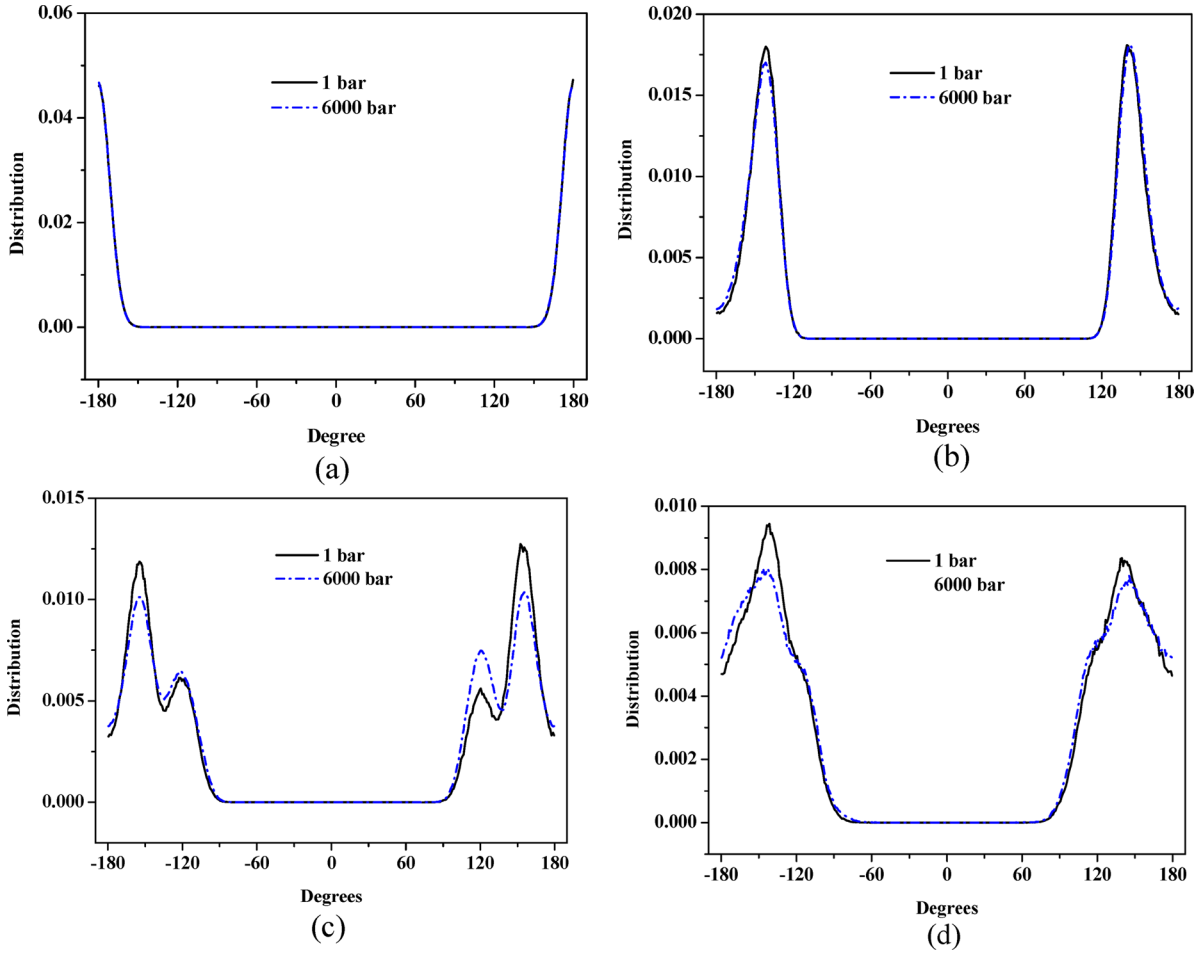

Figure 7. Distribution of the torsion angles at 1 and 6000 bar: (a) 4−5−1−7; (b) 4−5−1−8; (c) 4−5−1−9; (d) 4−5−1−10.

observed as the length of the alkyl chain increases as a result of the increased rotational freedom. Long alkyl long chains in asymmetric cations can result in aggregation via interdigitation or bilayer formation,[45] and should be compressed more easily under the influence of high pressure.[38]

3.3. Impact of Pressure on the Interaction and Properties of $[C_4mim][PF_6]$. *3.3.1. The Interaction Energy.* The electrostatic and LJ interaction energies for $[C_4mim][PF_6]$ at 313 K under different pressures are shown in Table 2. The data clearly indicate that electrostatic interactions dominate the system energy. The electrostatic interaction energies for cation−cation, anion−anion, and cation−anion all increase substantially with increasing pressure. The Lennard-Jones interaction energies decrease slightly from −74.2 to −78.0 kJ/mol. The data indicate that higher pressures enhance the interionic electrostatic interactions and the LJ interactions; however, the electrostatic interactions still dominate the interactions of ILs.

3.3.2. Cohesive Energy Density. The structural and interaction changes observed above can cause variations in the IL's properties. One of the most important properties of ILs is the cohesive energy density (*c*), which can be studied by the heat of evaporation (ΔH_{vap}) and their vapor pressure,[46] which are defined in eqs 2 and 3:

dx.doi.org/10.1021/jp3070568 | J. Phys. Chem. B 2012, 116, 10876−10884

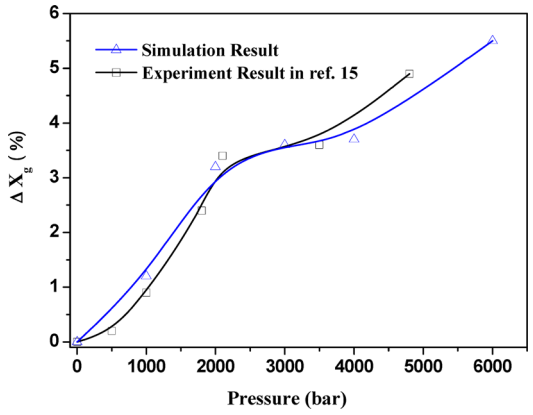

Figure 8. The increment ratio of the *g* conformer with increasing pressure: simulation result (triangles), experiment result from ref 15 (squares).

$$\Delta H^{\mathrm{vap}} = \Delta U^{\mathrm{vap}} + RT \tag{2}$$

$$c = \Delta U^{\mathrm{vap}}/V_{\mathrm{m}} \tag{3}$$

where R is the gas constant and V_{m} is the molar volume of the liquid. The above equations are both related to ΔU_{vap}, which represents the change of the internal energy after vaporization. It can be simplified by eq 4:

$$\Delta U^{\mathrm{vap}} = -U^{\mathrm{int}} + U^{\mathrm{ion\,pair}} \tag{4}$$

Table 3 presents the changes in internal energy for vaporization, intermolecular energies, heat of vaporization, molar volumes, and cohesive energy density at different pressures. The cohesive energy density of $[C_4mim][PF_6]$ increases with increasing pressure. As discussed above, pressure reduces the distance between the ions and distorts the butyl chains, resulting in the increased cohesive energy density. Such high cohesive energy density can enhance the interaction between the ions, and thus, other dynamics properties will also be affected by the high pressure.

3.3.3. Transport Properties. To explore the dynamic properties of $[C_4mim][PF_6]$, MSD, SDC, viscosity, and conductivity were studied at different pressures. The mobility of the ions was determined from the MSD of the center of mass of the ions (Figure 12), and it was found that the MSDs for both cation and anion decrease with increasing pressure, indicating that the mobility of the ions is reduced at high pressure. This is consistent with the enhancement of the interionic interactions by high pressure.

The coefficient of self-diffusion for a liquid can be calculated using the Einstein relation, eq 5:

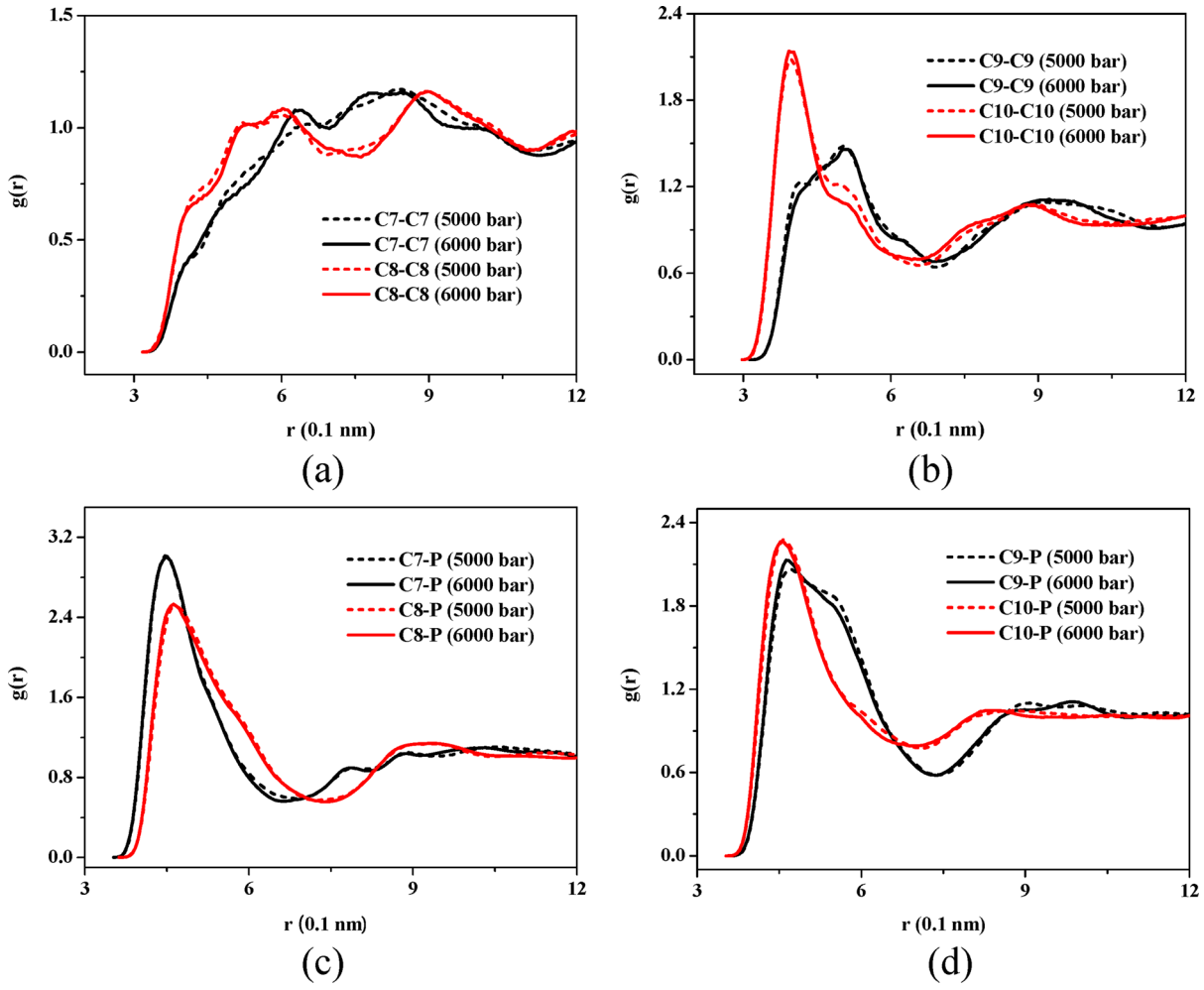

Figure 9. Pair−pair RDFs of C7−C7, C7−P, C8−C8, C8−P, C9−C9, C9−P, C10−C10, and C10−P at 5000 bar (dashed line) and 6000 bar (solid line).

dx.doi.org/10.1021/jp3070568 | J. Phys. Chem. B 2012, 116, 10876−10884

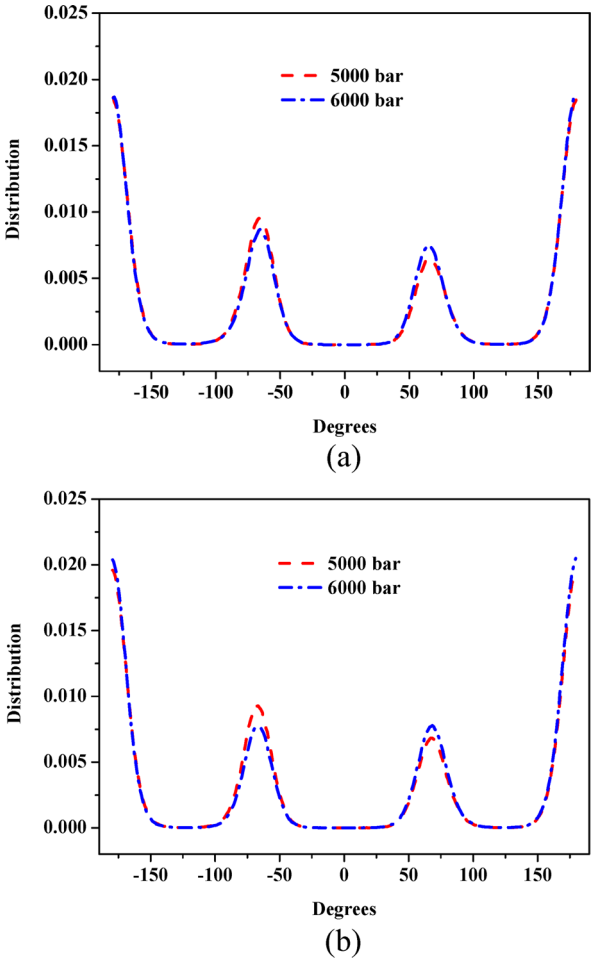

Figure 10. Distribution of torsion angles at 1 and 6000 bar for 1−7−8−9 (a) and 7−8−9−10 (b).

Table 1. Ratio of *a*, −*g*, and +*g* Configuration According to the First C7−C8 Bond and the Second C8−C9 Bond in the Cation

	C7−C8 bond			C8−C9 bond		
pressure (bar)	*a*	−*g*	+*g*	*a*	−*g*	+*g*
5000	0.603	0.205	0.192	0.546	0.231	0.223
6000	0.571	0.218	0.211	0.536	0.223	0.242

$$D = \frac{1}{6}\lim_{t\to\infty}\frac{\mathrm{d}}{\mathrm{d}t}\langle |ri(t) - ri(0)|^2\rangle \quad (5)$$

The quantity in braces is the ensemble-averaged MSD of the molecules and *ri* is the vector coordinate of the center of mass of ion *i*.

The SDC values of the cations and anions are shown in Table 4, where it can be observed that the SDC becomes smaller with increased pressure. Here again, the strong interactions between the cation and anion might account for the lower diffusion constant value of the ILs. This simulation result is consistent with the trend of the reported experimental data.[24]

Using the Stokes−Einstein relation, the viscosities of the ILs can be estimated with eq 6:

$$\eta_{IL} = \eta_{H_2O}\frac{D_{H_2O}}{D_{IL}} \quad (6)$$

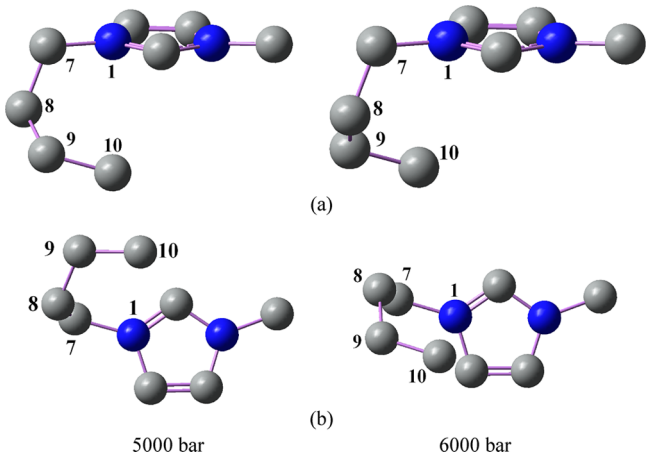

Figure 11. Snapshot of the structural change of one cation from 5000 to 6000 bar: (a) from the direction parallel to the ring and (b) from the direction perpendicular to the ring.

Table 2. Interionic Interactions for [C_4mim][PF_6] at 313 K

pressure (bar)	interaction	electrostatic interactions (kJ/mol)	Lennard-Jones interactions (kJ/mol)
1	cation−cation	4798.3	−74.2
	cation−anion	−9991.4	
	anion−anion	4761.5	
1000	cation−cation	4933.1	−75.9
	cation−anion	−10262.1	
	anion−anion	4896.0	
3000	cation−cation	5144.3	−77.9
	cation−anion	−10684.2	
	anion−anion	5105.8	
6000	cation−cation	5341.8	−78.0
	cation−anion	−11081.8	
	anion−anion	5302.2	

Table 3. U^{int}, ΔH^{vap}, V_m, and *C* of [C_4mim][PF_6] at Different Pressures[a]

pressure (bar)	ΔU^{vap} (kJ/mol)	U^{int} (kJ/mol)	ΔH^{vap} (kJ/mol)	V_m (cm^3/mol)	*C* (J/cm^3)
1	182.2	−505.8	184.8	210.2	866.8
1000	185.3	−508.9	187.9	204.6	905.4
3000	188.4	−512.0	191.0	196.6	958.5
6000	192.2	−515.8	194.8	189.4	1014.9

[a] ΔU^{vap}, internal energies for vaporization; U^{int}, intermolecular energies; ΔH^{vap}, the heat of evaporation; V_m, molar volume of the liquid; *C*, cohesive energy density.

where $D_{IL} = 1/2(D_{cation} + D_{anion})$ and η_{H_2O}= 0.9 mPa·s^{-1}.[47] From these results (Table 4), it is clear that, as expected, the viscosity increases with increasing pressure.

To confirm the validity of the calculation, the viscosity observed at 313 K and 1 bar was compared with an

dx.doi.org/10.1021/jp3070568 | J. Phys. Chem. B 2012, 116, 10876−10884

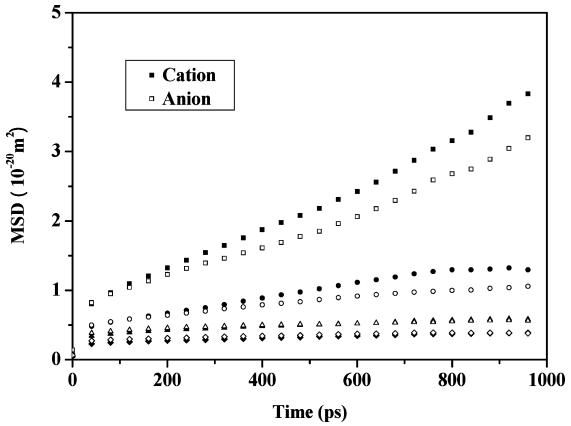

Figure 12. Average mean square displacements of $[C_4mim][PF_6]$ at different pressures at 313 K: cation (open symbols), anion (filled symbols), 1 bar (squares), 1000 bar (circles), 3000 bar (triangles), 6000 bar (diamonds).

experimental result. The calculated viscosity of $[C_4mim][PF_6]$ at 313 K is 0.52 Pa·s^{-1} at 1 bar, which can be compared to the experimental value of 0.12 Pa·s^{-1} at 313 K.[43] The difference may arise from the difficulty in calculating transport properties in such short time scales. Most of the ions in ILs move very slowly, and it is difficult to obtain data in good agreement with experimental data when computed on the order of several nanoseconds. Of course, one must also be aware that many experimental data are complicated by impurities which may interfere with exact measurements of physical properties.[48]

Estimates of the molar conductivity for ILs can be obtained from the Nernst–Einstein equation[49,50] (eq 7):

$$\Lambda_{IL} = \frac{N_A e^2}{k_B T}(D_{cation} + D_{anion}) \quad (7)$$

where N_A is Avogadro's number and e is the electron charge. The estimated molar conductivities Λ_{IL} and conductivities κ_{IL} for $[C_4mim][PF_6]$ are listed in Table 4. The simulation results showed that the conductivity decreases with increasing pressure. Kanakubo et al.[24] measured the electrical conductivity under high pressure up to 2000 bar and reported that the conductivities of $[C_4mim][PF_6]$ at 300 K under normal pressure and 1000 bar are 0.1444 and 0.0429 S·m^{-1}, respectively. Compared with the experimental results, our simulation results would seem to have some error; however, the simulation data have the same order of magnitude and trends as the experimental values.

4. CONCLUSIONS

In this paper, the changes in structure and properties of $[C_4mim][PF_6]$ as a function of pressure were simulated. RDF and torsion angle data indicated changes in the butyl chain where 5.5% of the *a* conformer converted to the *g* conformer according to the deformation of the alkyl chain at 6000 bar. A small jump was observed in the density change from 5000 to 6000 bar, which could be attributed to the fact that the positions of C9 and C10 in the *g* conformer around C7–C8 and C8–C9 bonds reversed direction to reduce the overall spatial volume under this range of pressure.

The structural changes of $[C_4mim][PF_6]$ under high pressure change the ion interactions and overall properties. The intermolecular electrostatic interactions and the LJ interactions are enhanced by pressure, while the calculated cohesive energies of this IL increase gradually with increasing pressure. The diffusion of the IL and estimated conductivities are reduced and the viscosity is enhanced dramatically. These results are in accordance with experimental findings and provide a theoretical foundation for the experimental investigations and for future applications of ionic liquids under high pressure.

■ ASSOCIATED CONTENT

Supporting Information

Table showing the liquid densities for $[C_4mim][PF_6]$ at different pressures with different simulated conditions. This material is available free of charge via the Internet at http://pubs.acs.org.

■ AUTHOR INFORMATION

Corresponding Author

*E-mail: xmlu@home.ipe.ac.cn (X.L.); jwang@henannu.edu.cn (J.W.); rdrogers@as.ua.edu (R.D.R.).

Notes

The authors declare no competing financial interest.

■ ACKNOWLEDGMENTS

This work was supported by National Basic Research Program of China (2009CB219902) and the National Natural Science Foundation of China (Grant Nos. 20976174 and 20903098) and State Key Laboratory of Multiphase Complex Systems (MPCS-2011-D-05).

■ REFERENCES

(1) Adam, D. *Nature* **2000**, *407*, 938.
(2) Welton, T. *Chem. Rev.* **1999**, *99*, 2071.
(3) Rogers, R.; Seddon, K. *Science* **2003**, *302*, 792.
(4) Wasserscheid, P.; Keim, W. *Angew. Chem., Int. Ed.* **2000**, *39*, 3773.
(5) Dean, P.; Turanjanin, J.; Yoshizawa-Fujita, M.; MacFarlane, D.; Scott, J. *Cryst. Growth Des.* **2009**, *9*, 1137.
(6) Wojnarowska, Z.; Wlodarczyk, P.; Kaminski, K.; Grzybowska, K.; Hawelek, L.; Paluch, M. *J. Chem. Phys.* **2010**, *133*, 094507.
(7) Sun, N.; Rahman, M.; Qin, Y.; Maxim, M.; Rodriguez, H.; Rogers, R. *Green Chem.* **2009**, *11*, 646.
(8) Xu, A.; Wang, J.; Wang, H. *Green Chem.* **2010**, *12*, 268.
(9) Trombetta, F.; de Souza, M.; de Souza, R.; Martini, E. *J. Appl. Electrochem.* **2009**, *39*, 2315.
(10) Imai, Y.; Abe, H.; Goto, T.; Takekiyo, T.; Yoshimura, Y. *High Pressure Res.* **2009**, *29*, 536.

Table 4. Transport Properties for $[C_4mim][PF_6]$

pressure (bar)	D_{cation} (10^{-12} m^2/s)	D_{anion} (10^{-12} m^2/s)	D_{IL} (10^{-12} m^2/s)	η_{IL} (Pa·s)	Λ_{IL} (10^{-5} S·m^2/mol)	κ_{IL} (10^{-2} S/m)
1	4.7	3.6	4.2	0.52	3.0	14
1000	1.8	1.2	1.5	1.4	1.1	5.3
3000	0.39	0.24	0.32	6.6	0.23	1.2
6000	0.29	0.25	0.27	7.8	0.19	1.0

(11) Zhao, Y.; Dong, K.; Liu, X.; Zhang, S.; Zhu, J.; Wang, J. *Mol. Simul.* **2012**, *38*, 172.
(12) English, N.; Mooney, D. *Phys. Chem. Chem. Phys.* **2009**, *11*, 9370.
(13) Su, L.; Li, M.; Zhu, X.; Wang, Z.; Chen, Z.; Li, F.; Zhou, Q.; Hong, S. *J. Phys. Chem. B* **2010**, *114*, 5061.
(14) Su, L.; Li, L.; Hu, Y.; Yuan, C.; Shao, C.; Hong, S. *J. Chem. Phys.* **2009**, *130*, 184503.
(15) Russina, O.; Fazio, B.; Schmidtc, C.; Triolo, A. *Phys. Chem. Chem. Phys.* **2011**, *13*, 12067.
(16) Domanska, U.; Morawski, P. *Green Chem.* **2007**, *9*, 361.
(17) Salvador, A.; Santos, M.; Saraiva, J. *Green Chem.* **2010**, *12*, 632.
(18) Rivera-Calzada, A.; Kaminski, K.; Leon, C.; Paluch, M. *J. Phys. Chem. B* **2008**, *112*, 3110.
(19) Yoshimura, Y.; Takekiyo, T. *J. Phys. Chem. C* **2012**, *116*, 2097.
(20) Chang, H.; Jiang, J.; Su, J.; Chang, C.; Lin, S. *J. Phys. Chem. A* **2007**, *111*, 9201.
(21) Chang, H.; Jiang, J.; Chang, C.; Su, J.; Hung, C.; Liou, Y.; Lin, S. *J. Phys. Chem. B* **2008**, *112*, 4351.
(22) Imai, Y.; Takekiyo, T.; Abe, H.; Yoshimura, Y. *High Pressure Res.* **2010**, *31*, 53.
(23) Takekiyo, T.; Imai, Y.; Hatano, N.; Abe, H.; Yoshimura, Y. *High Pressure Res.* **2010**, *31*, 35.
(24) Kanakubo, M.; Harris, K.; Tsuchihashi, N.; Ibuki, K.; Ueno, M. *J. Phys. Chem. B* **2007**, *111*, 2062.
(25) Harris, K.; Kanakubo, M.; Tsuchihashi, N.; Ibuki, K.; Ueno, M. *J. Phys. Chem. B* **2008**, *112*, 9830.
(26) Morrow, T.; Maginn, E. *J. Phys. Chem. B* **2002**, *106*, 12807.
(27) Liu, Z.; Huang, S.; Wang, W. *J. Phys. Chem. B* **2004**, *108*, 12978.
(28) Liu, Z.; Chen, T.; Bell, A.; Smit, B. *J. Phys. Chem. B* **2010**, *114*, 4572.
(29) Canongia Lopes, J.; Pádua, A. *J. Phys. Chem. B* **2006**, *110*, 7485.
(30) Bhargavaa, B.; Balasubramanianb, S. *J. Chem. Phys.* **2007**, *127*, 114510.
(31) Micaelo, N.; Baptista, A.; Soares, C. *J. Phys. Chem. B* **2006**, *110*, 14444.
(32) Zhao, W.; Leroy, F.; Heggen, B.; Zahn, S.; Kirchner, B.; Balasubramanian, S.; Müller-Plathe, F. *J. Am. Chem. Soc.* **2009**, *131*, 15825.
(33) Sarangi, S.; Zhao, W.; Müller-Plathe, F.; Balasubramanian, S. *ChemPhysChem* **2010**, *11*, 2001.
(34) Aragones, J.; Conde, M.; Noya, E.; Vega, C. *Phys. Chem. Chem. Phys.* **2009**, *11*, 543.
(35) Kohno, Y.; Hiyoshi, R.; Yamaguchi, Y.; Matsumoto, S.; Koseki, A.; Takahashi, O.; Yamasaki, K.; Ueda, K. *J. Phys. Chem. A* **2009**, *113*, 2551.
(36) Meher, B.; Satish Kumar, M.; Sen, K. *Proc. 11th Internat. Conf. on Information Techno.* **2008**, 118.
(37) Velardez, G.; Alavi, S.; Thompsona, D. *J. Chem. Phys.* **2003**, *119*, 6698.
(38) Shah, J.; Maginn, E. *Fluid Phase Equilib.* **2010**, *294*, 197.
(39) Lyubartsev, A.; Laaksonen, A. *Comput. Phys. Commun.* **2000**, *128*, 565.
(40) Liu, X.; Zhao, Y.; Zhang, X.; Zhou, G.; Zhang, S. *J. Phys. Chem. B* **2012**, *116*, 4934.
(41) Martyna, G.; Tuckerman, M.; Tobias, D.; Klein, M. *Mol. Phys.* **1996**, *87*, 1117.
(42) Su, L.; Zhu, X.; Wang, Z.; Cheng, X.; Wang, Y.; Yuan, C.; Chen, Z.; Ma, C.; Li, F.; Zhou, Q.; Cui, Q. *J. Phys. Chem. B* **2012**, *116*, 2216.
(43) Zhang, S.; Sun, N.; He, X.; Lu, X.; Zhang, X. *J. Phys. Chem. Ref. Data* **2006**, *35*, 1475.
(44) Endo, T.; Kato, T.; Tozaki, K.; Nishikawa, K. *J. Phys. Chem. B* **2010**, *114*, 407.
(45) Wang, J.; Wang, H.; Zhang, S.; Zhang, H.; Zhao, Y. *J. Phys. Chem. B* **2007**, *111*, 6181.
(46) Liu, X.; Zhang, S.; Zhou, G.; Wu, G.; Yuan, X.; Yao, X. *J. Phys. Chem. B* **2006**, *110*, 12062.
(47) Liu, X.; Zhou, G.; Zhang, S.; Wu, G.; Yu, G. *J. Phys. Chem. B* **2007**, *111*, 5658.
(48) Kelkar, M. S.; Maginn, E. J. *J. Phys. Chem. B* **2007**, *111*, 4867.
(49) Margulis, C.; Stern, H.; Berne, B. *J. Phys. Chem. B* **2002**, *106*, 12017.
(50) Noda, A.; Hayamizu, K.; Watanabe, M. *J. Phys. Chem. B* **2001**, *105*, 4603.